

University of Groningen

Sensitivity of nonequilibrium Casimir forces on low frequency optical properties toward chaotic motion of microsystems

Tajik, F.; Masoudi, A. A.; Babamahdi, Z.; Sedighi, M.; Palasantzas, G.

Published in:
Chaos

DOI:
[10.1063/1.5140076](https://doi.org/10.1063/1.5140076)

IMPORTANT NOTE: You are advised to consult the publisher's version (publisher's PDF) if you wish to cite from it. Please check the document version below.

Document Version
Publisher's PDF, also known as Version of record

Publication date:
2020

[Link to publication in University of Groningen/UMCG research database](#)

Citation for published version (APA):

Tajik, F., Masoudi, A. A., Babamahdi, Z., Sedighi, M., & Palasantzas, G. (2020). Sensitivity of nonequilibrium Casimir forces on low frequency optical properties toward chaotic motion of microsystems: Drude vs plasma model. *Chaos*, 30(2), [023108]. <https://doi.org/10.1063/1.5140076>

Copyright

Other than for strictly personal use, it is not permitted to download or to forward/distribute the text or part of it without the consent of the author(s) and/or copyright holder(s), unless the work is under an open content license (like Creative Commons).

The publication may also be distributed here under the terms of Article 25fa of the Dutch Copyright Act, indicated by the "Taverne" license. More information can be found on the University of Groningen website: <https://www.rug.nl/library/open-access/self-archiving-pure/taverne-amendment>.

Take-down policy

If you believe that this document breaches copyright please contact us providing details, and we will remove access to the work immediately and investigate your claim.

Downloaded from the University of Groningen/UMCG research database (Pure): <http://www.rug.nl/research/portal>. For technical reasons the number of authors shown on this cover page is limited to 10 maximum.


Sensitivity of nonequilibrium Casimir forces on low frequency optical properties toward chaotic motion of microsystems: Drude vs plasma model

Cite as: Chaos **30**, 023108 (2020); <https://doi.org/10.1063/1.5140076>

Submitted: 25 November 2019 . Accepted: 14 January 2020 . Published Online: 03 February 2020

F. Tajik, A. A. Masoudi, Z. Babamahdi, M. Sedighi, and G. Palasantzas 

COLLECTIONS

 This paper was selected as Featured



View Online



Export Citation



CrossMark

ARTICLES YOU MAY BE INTERESTED IN

[Dependence of non-equilibrium Casimir forces on material optical properties toward chaotic motion during device actuation](#)

Chaos: An Interdisciplinary Journal of Nonlinear Science **29**, 093126 (2019); <https://doi.org/10.1063/1.5124308>

[Motor execution reduces EEG signals complexity: Recurrence quantification analysis study](#)

Chaos: An Interdisciplinary Journal of Nonlinear Science **30**, 023111 (2020); <https://doi.org/10.1063/1.5136246>

[Totally asymmetric simple exclusion process on multiplex networks](#)

Chaos: An Interdisciplinary Journal of Nonlinear Science **30**, 023103 (2020); <https://doi.org/10.1063/1.5135618>

Scilight Highlights of the best new research
in the **physical sciences**

[LEARN MORE!](#)



Sensitivity of nonequilibrium Casimir forces on low frequency optical properties toward chaotic motion of microsystems: Drude vs plasma model

Cite as: Chaos 30, 023108 (2020); doi: 10.1063/1.5140076

Submitted: 25 November 2019 · Accepted: 14 January 2020 ·

Published Online: 3 February 2020



View Online



Export Citation



CrossMark

F. Tajik,^{1,2} A. A. Masoudi,¹ Z. Babamahdi,² M. Sedighi,³ and G. Palasantzas^{2,a)} 

AFFILIATIONS

¹Department of Physics, Alzahra University, Tehran 1993891167, Iran

²Zernike Institute for Advanced Materials, University of Groningen, Nijenborgh 4, 9747 AG Groningen, The Netherlands

³Department of Mechanical Engineering, University of Sistan and Baluchestan, Zahedan, Iran

^{a)}Author to whom correspondence should be addressed: g.palasantzas@rug.nl

ABSTRACT

Here, we investigate the sensitivity of nonequilibrium Casimir forces to optical properties at low frequencies via the Drude and plasma models and the associated effects on the actuation of microelectromechanical systems. The stability and chaotic motion for both autonomous conservative and nonconservative driven systems were explored assuming good, e.g., Au, and poor, e.g., doped SiC, interacting conductors having large static conductivity differences. For both material systems, we used the Drude and plasma methods to model the optical properties at low frequencies, where measurements are not feasible. In fact, for the conservative actuating system, bifurcation and phase space analysis show that the system motion is strongly influenced by the thermal nonequilibrium effects depending on the modeling of the optical properties at low frequencies, where also the presence of residual electrostatic forces can also drastically alter the actuating state of the system, depending strongly on the material conductivity. For nonconservative systems, the Melnikov function approach is used to explore the presence of chaotic motion rendering predictions of stable actuation or malfunction due to stiction on a long-term time scale rather impossible. In fact, the thermal effects produce the opposite effect for the emerging chaotic behavior for the Au–Au and SiC–SiC systems if the Drude model is used to model the low optical frequencies. However, using the plasma model, only for the poor conducting SiC–SiC system, the chance of chaotic motion is enhanced, while for the good conducting Au–Au system, the chaotic behavior will remain unaffected at relatively short separations ($<2 \mu\text{m}$).

Published under license by AIP Publishing. <https://doi.org/10.1063/1.5140076>

Advancement in microfabrication techniques has driven significant attention to micro-(MEMS) and nanoelectromechanical (NEMS) systems from both the fundamental science and technology point of view. In order to analyze in depth the functionality of devices at micrometer/submicrometer separations, it is vital to consider Casimir forces since they are omnipresent and inevitably can influence the dynamics of moving components. It is of primary importance to understand under what conditions this force can draw moving elements together into permanent adhesion, which is termed as stiction. Furthermore, the occurrence of chaotic behavior is unavoidable, and it can cause abrupt changes in actuation leading to possible stiction

during the long-term performance of devices. This is strongly dependent on the magnitude of the Casimir force, in both equilibrium and non-equilibrium conditions, where the latter case takes place generally in a system with components at different temperature. The situation becomes more complicated by the uncertainty in calculating the Casimir force, which is known for more than 15 years now, due to the extrapolation of the measured optical properties at low frequencies via the Drude or the plasma (P) models. The latter model can predict either enhanced or suppressed chaotic behavior depending strongly also on the conductivity of the interacting materials.

I. INTRODUCTION

Nowadays, microelectromechanical systems (MEMS) are becoming increasingly an important element for various technology applications such as microswitches, accelerometers, sensors, microphones, etc. Attracting attention to this sort of devices at the micrometer and submicrometer length scales has driven significant advancement in microfabrication techniques, which lead to scaling down of MEMS into submicrometer length scales toward nanoelectromechanical systems (NEMS).^{1–9} As a result, these processes lead inevitably to a significant role for the Casimir force on the actuation dynamics of the devices.^{1–9} Although electrostatic actuation has been utilized in micro/nanodevices, the electrostatic forces can be switched off when no potential is applied. However, the Casimir force is omnipresent, and it can always influence the actuation dynamics of operating devices. This is because MEMS/NEMS have surface areas large enough and separation gaps small enough for the Casimir force to play a significant role and under certain conditions to pull mechanical elements together leading to permanent adhesion, which is known as stiction.^{2,8,9}

The Casimir force was predicted by H. Casimir in 1948 when he assumed that two perfectly conducting parallel plates are attracting each other due to the perturbation of vacuum fluctuations of the electromagnetic (EM) field.¹⁰ Later on, Lifshitz and co-workers¹¹ considered the general case of real dielectric plates by exploiting the fluctuation–dissipation theorem, which relates the dissipative properties of the plates (optical absorption by many microscopic dipoles) and the resulting EM fluctuations. The Lifshitz theory predicts the Casimir force between two plates for any material and covers both the short-range (nonretarded) van der Waals and the long-range (retarded) Casimir asymptotic regimes, respectively.^{1–4,10–13} Furthermore, in order to analyze the dynamical behavior of MEMS operating under ambient conditions between materials with different conductivities, several studies have shown so far how the optical properties^{14–24} and thermal nonequilibrium effects^{25–28} can influence their motion. These results allow one to tailor the force by a suitable choice of interacting materials at an appropriate temperature, opening new possibilities for MEMS/NEMS engineering.

Moreover, it has been shown that the low optical frequency range, which is not accessible by experimental measurements,^{14–24} is playing a significant role for an effective stable operation of devices.^{3,4,29–31} In fact, Casimir force measurements have revealed deviations from force predictions of dissipative models (e.g., the Drude model),^{3,4,30} which lead to finite absorption at frequencies $\omega > 0$ and singular absorption $\sim 1/\omega$ for $\omega \rightarrow 0$ (static limit). On the other hand, the plasma (P) model,^{3,4,30} which can also be thought as having infinite absorption at the frequency $\omega \sim 0$, and zero anywhere else, allowed calculations of the Casimir force that described the measured force data more precisely at separations above 160 nm.^{3,4,30,31} Recently, we have shown that for systems at thermal equilibrium, the choice of the Drude or plasma models to describe the optical properties at low optical frequencies (far-infrared and below) in the range where any measured optical data are not available leads to remarkably different results regarding the stability and emerging chaotic motion of MEMS.^{29,31}

However, it is still remains unexplored how the optical properties in the low frequency range can affect the actuation of

devices towards chaotic motion under the influence of thermal nonequilibrium Casimir forces taking into account the conductivity of interacting materials, and possible residual electrostatic interactions due to uncompensated contact potentials. This topic will be explored here for both good and poor conductive materials that are used in microdevices and can lead to irreversible adhesion of moving parts due to stiction on a long-term during operation. In fact, the design of these devices can always be quite challenging due to the occurrence of chaotic behavior, which causes abrupt changes in their dynamical behavior resulting in device malfunction. As a result, the present study will provide essential knowledge for the design of actuating devices operating under nonequilibrium conditions and add new functionalities to MEMS/NEMS architectures taking into account detailed modeling of material optical properties.

II. MATERIAL SYSTEMS AND DEVICE ACTUATION

For our purpose, we have chosen gold (Au) and highly doped silicon carbide (SiC) in order to cover a wide range of materials with different optical properties and associated conductivities. Au is used due to its high conduction ratio $\omega_p^2/\omega_\tau|_{\text{Au}} 1600 \text{ eV}^{19}$ and its frequent use in devices, while as a poor conductor, we used nitrogen doped SiC with a conductivity ratio of $\omega_p^2/\omega_\tau|_{\text{SiC}} = 0.4 \text{ eV}^{24}$. Notably, SiC is also suitable for operation in harsh environments and an important system that is compatible with Si-based technologies. Both materials were optically characterized with the same ellipsometric equipment [J. A. Woollam Co., Inc., ellipsometers VUV-VASE (0.5–9.34 eV) and IR-VASE (0.03–0.5 eV)].^{19,24} Details for the Drude and plasma models and the frequency dependent dielectric functions of the materials in our study are shown in Appendix A. The corresponding dielectric functions at imaginary frequencies $\epsilon(i\xi)$, which are the necessary inputs for calculating the contribution of the zero-point fluctuations ($T = 0$) on the Casimir force via the Lifshitz theory, are calculated as explained in Appendix A.^{19,24,31}

In order to understand the influence of the nonequilibrium Casimir force on MEMS actuation, we have considered in Fig. 1 a typical microswitch, which is a well-known essential device. It

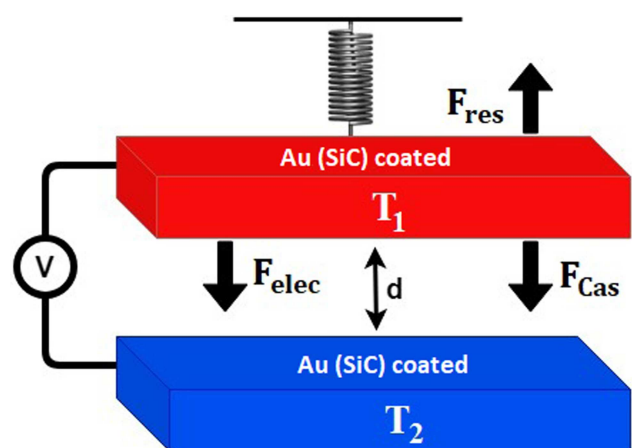


FIG. 1. Schematic of the model actuating system under consideration.

is constructed from two electrodes of which one is fixed, and the other is suspended by a mechanical spring governed by Hooke's law.³² The elastic restoring force $F_{\text{res}} = k(d - z)$ of the spring with stiffness k counterbalances both the attractive Casimir and electrostatic forces. After applying a bias voltage V between the planar electrodes and/or due to the uncompensated contact potentials of the material coatings, an electrostatic force F_{elec} is produced,

$$F_{\text{elec}}(z) = \frac{\epsilon_0 AV^2}{2z^2}, \quad (1)$$

where ϵ_0 is the permittivity of vacuum between the plates. Furthermore, it is possible to express the nonequilibrium Casimir force F_{Cas} between the plates as

$$F_{\text{Cas}}(T_1, T_2, z) = F_0(z) + F_{\text{th}}^{\text{neq}}(T_1, T_2, z), \quad (2)$$

where the contribution of the zero-point fluctuations ($T = 0$) $F_0(z)$ is separated from the thermal part $F_{\text{th}}^{\text{neq}}(T_1, T_2, z)$ due to thermal fluctuations. $F_0(z)$ has been calculated via the Lifshitz theory using the dielectric functions at imaginary frequencies $\epsilon(i\xi)$ for both the Drude and plasma models (see Appendix A for the extrapolations of the measured optical data via the Drude and plasma models). The chosen materials (Au and SiC) show significant optical contrast for the dielectric function at imaginary frequencies $\epsilon(i\xi)$ at frequencies of $\xi < 1$ eV, which will manifest in Casimir force variations for nanoscale separations $c/2\xi > 10$ nm.

According to Ref. 25, the thermal force between the two bodies in both configurations in and out of thermal equilibrium can be presented as

$$F_{\text{th}}^{\text{neq}}(T_1, T_2, z) = F_{\text{th}}^{\text{neq}}(T_1, 0, z) + F_{\text{th}}^{\text{neq}}(0, T_2, z). \quad (3)$$

The first and the second term at the right side of Eq. (3) describe the bodies at temperature T_1 and T_2 , respectively. This part for each body can be written as

$$F_{\text{th}}^{\text{neq}}(T, z) = F_{\text{th}}^{\text{neq PW}}(T, z) + F_{\text{th}}^{\text{neq EW}}(T, z). \quad (4)$$

Equations (2)–(4) can be presented using the Lifshitz formula in real frequencies as a sum of contributions from propagating and evanescent waves. The propagating waves satisfy the condition $ck_{\perp} < \omega$, (k_{\perp} is the in-plane wave vector), which is valid for real photons. They propagate both in the vacuum gap and inside the bodies. The corresponding out of plane wave vector k_0 is real. Evanescent waves satisfy the condition $\omega \leq ck_{\perp}$, and they may propagate only along the boundary planes. The electromagnetic field of an evanescent wave decreases exponentially with the distance from the interface between the vacuum gap and the interacting bodies, and the corresponding out of plane wave vector k_0 is imaginary.

In this study, our main goal is to investigate the influence of optical properties at low frequencies on the dynamical actuation of systems with strong and weak conductivity. Therefore, we have focused on identical interacting bodies and ignored mix states between good and poor conductors. The latter is highly interesting but will be given elsewhere for several systems including Au, SiC, Ru, and phase change materials. Moreover, the consideration of identical bodies simplifies the process of calculations to gain better insights into these complex situations. Indeed, according to Ref. 25, $F_{\text{th}}^{\text{neq}}(T, z)$ can be separated in symmetric and antisymmetric parts,

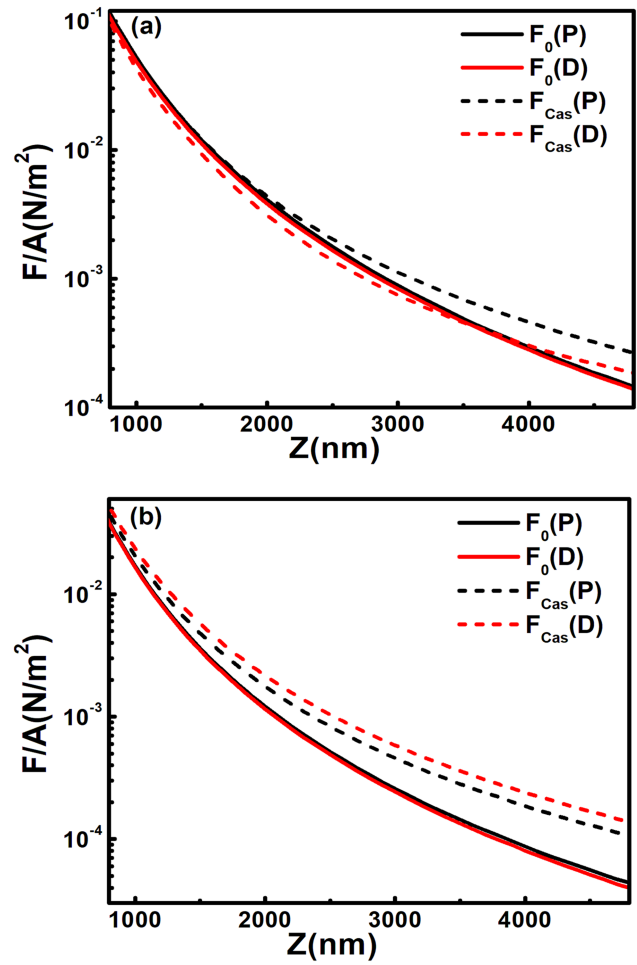


FIG. 2. Comparison between F_0 (zero-point fluctuations) and the $F_{\text{Cas}} (= F_0 + F_{\text{thermal}})$ for the (a) Au–Au and (b) SiC–SiC systems using both the Drude and plasma models. The calculations for the thermal contribution F_{thermal} were performed under nonequilibrium conditions for $T_1 = 300$ K and $T_2 = 400$ K.

where in a system with identical bodies the antisymmetric terms disappear (see Appendix B).

Finally, the equation of motion for the microelectromechanical system (Fig. 1), where the fixed and moving plates are considered to be coated by Au or SiC, is given by

$$M \frac{d^2 z}{dt^2} + \left(\frac{M\omega_0}{Q} \right) \frac{dz}{dt} = -F_{\text{res}} + F_{\text{elec}} + F_{\text{Cas}} + \epsilon F_0 \cos(\omega t). \quad (5)$$

Here $\epsilon F_0 \cos(\omega t)$ is the driven actuating force, M is the mass of the moving plate, and $(M\omega_0/Q)(dz/dt)$ is the intrinsic energy dissipation in the actuating system. For conservative systems, we consider actuating systems with a high quality factor $Q > 10^{433}$ so that we can neglect dissipation effects. The frequency ω_0 is assumed to be that of the dynamic mode atomic force microscope (AFM) cantilevers or MEMS (typically $\omega/2\pi = 3 \times 10^5$ rad/s).³³ The

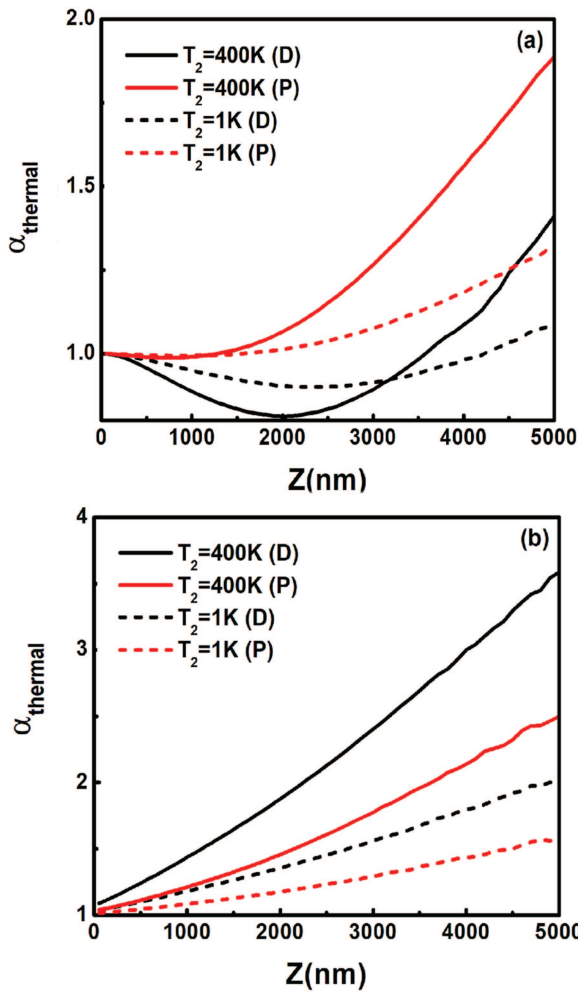


FIG. 3. $\alpha_{\text{thermal}} = F_{\text{Cas}}/F_0$ vs z for nonequilibrium conditions for the (a) Au–Au and (b) SiC–SiC systems using the Drude and plasma models.

parameter ϵ was introduced to distinguish between the conservative frictionless autonomous operation of the actuating system ($\epsilon = 0$) and the nonconservative driven system by an external force ($\epsilon = 1$) in the presence of friction having a finite quality factor Q . Finally, in each case, we assumed flat surfaces, because any nanoscale roughness will give significant contribution at separations below 100 nm,¹⁷ while we have considered different initial distances between the plates in the range $d = 850 \text{ nm}$ to $2.5 \mu\text{m}$. In all cases, the lateral dimensions of the plates were $L_x = L_y = 10 \mu\text{m}$.

III. RESULTS AND DISCUSSION

A. Conservative systems ($\epsilon = 0$)

For our stability analysis, we introduced the bifurcation parameter $\delta_{\text{Cas}} = F_{\text{Cas}}^{\text{m}/kd}$,^{34–36} which is the ratio of the minimum of Casimir force $F_{\text{Cas}}^{\text{m}} = F_{\text{Cas}}(z = d)$ to the maximum restoring force

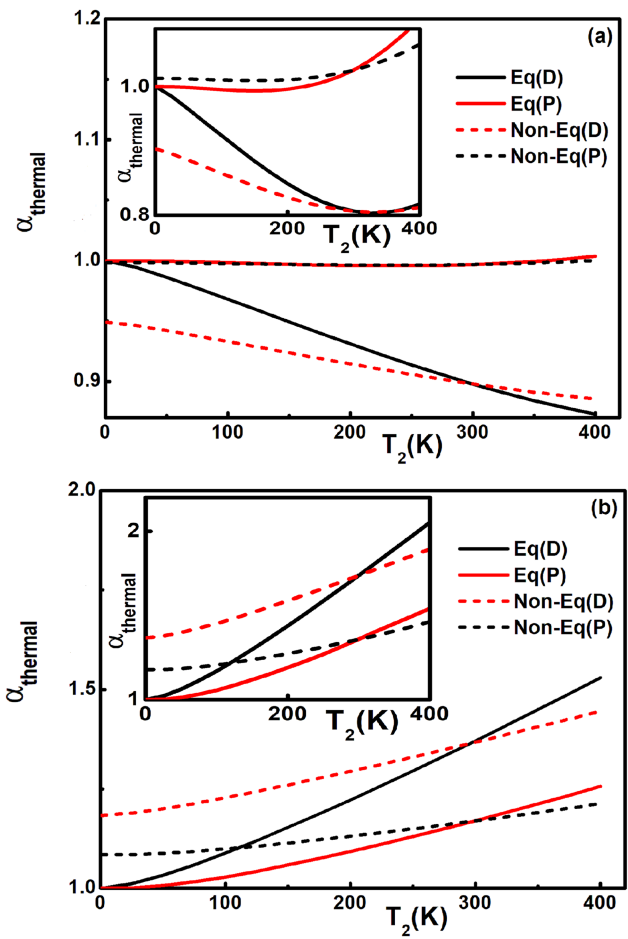


FIG. 4. $\alpha_{\text{thermal}} = F_{\text{Cas}}/F_0$ vs $T_2(\text{K})$ for both equilibrium ($T_1 = T_2$) and nonequilibrium ($T_1 = 300 \text{ K}$) situations in (a) Au–Au and (b) SiC–SiC systems using the Drude and plasma models. The separation distance between plates is $z = 1 \mu\text{m}$, while that in the inset is $z = 2 \mu\text{m}$.

kd. In this way, we are able to compare the force influence for different nonequilibrium thermal conditions. The locus of the equilibrium points is obtained from Eq. (5) if we set $F_{\text{total}} = -F_{\text{res}} + F_{\text{elec}} + F_{\text{Cas}} = 0$. The solution yields for the bifurcation parameter δ_{Cas} ^{35–37}

$$\delta_{\text{Cas}} = \left(-F_{\text{res}}(z) + \delta_v \frac{F_{\text{elec}}(z)}{F_{\text{elec}}^{\text{m}}} \right) \left(\frac{F_{\text{Cas}}^{\text{m}}}{F_{\text{Cas}}(z, T)} \right), \quad (6)$$

where $\delta_v = F_{\text{elec}}^{\text{m}}/F_{\text{res}}^{\text{m}} = \epsilon_0 AV^2/2kd^3$ is the corresponding electrostatic bifurcation parameter.^{21,38} The critical points, where stiction occurs, are also characterized by the condition $dF_{\text{total}}/dz = 0$.^{35–37} Therefore, the use of δ_{Cas} allows to determine when there is a stable periodic solution for the device that corresponds to sufficient restoring force to prevent stiction of the plates.³⁵ Using

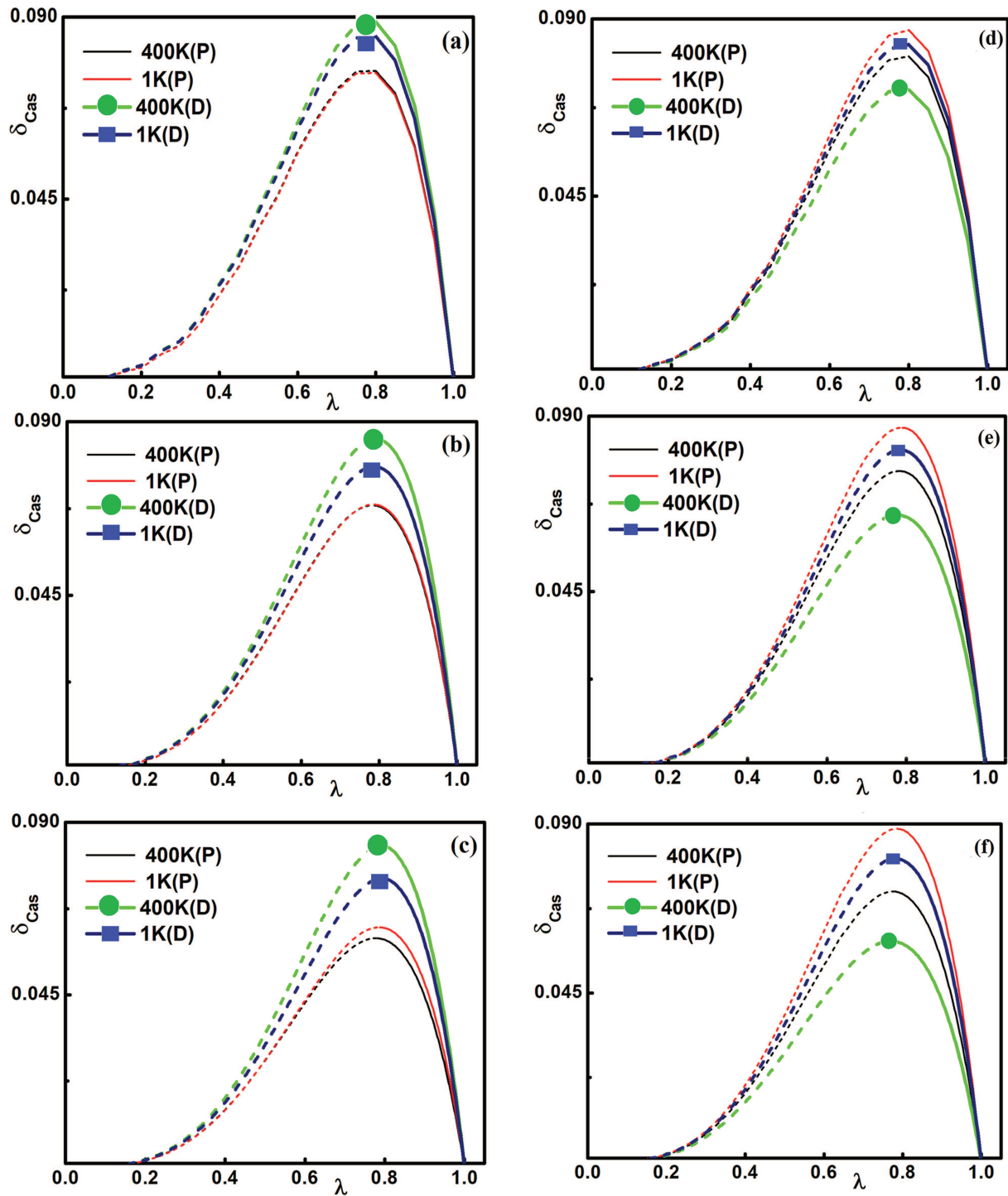


FIG. 5. Bifurcation diagrams δ_{Cas} vs λ ($= z/d$) for nonequilibrium conditions ($T_1 = 300$ K, $T_2 = 1$ K and 400 K), $\delta_v = 0$, and different initial actuation distances d : (a) $d = 850$ nm, (b) $d = 1$ μ m, and (c) $d = 2.5$ μ m for the Au–Au system; (d) $d = 850$ nm, (e) $d = 1$ μ m, and (f) $d = 2.5$ μ m for the SiC–SiC system. The solid and dashed lines represent the unstable and stable equilibrium points, respectively.

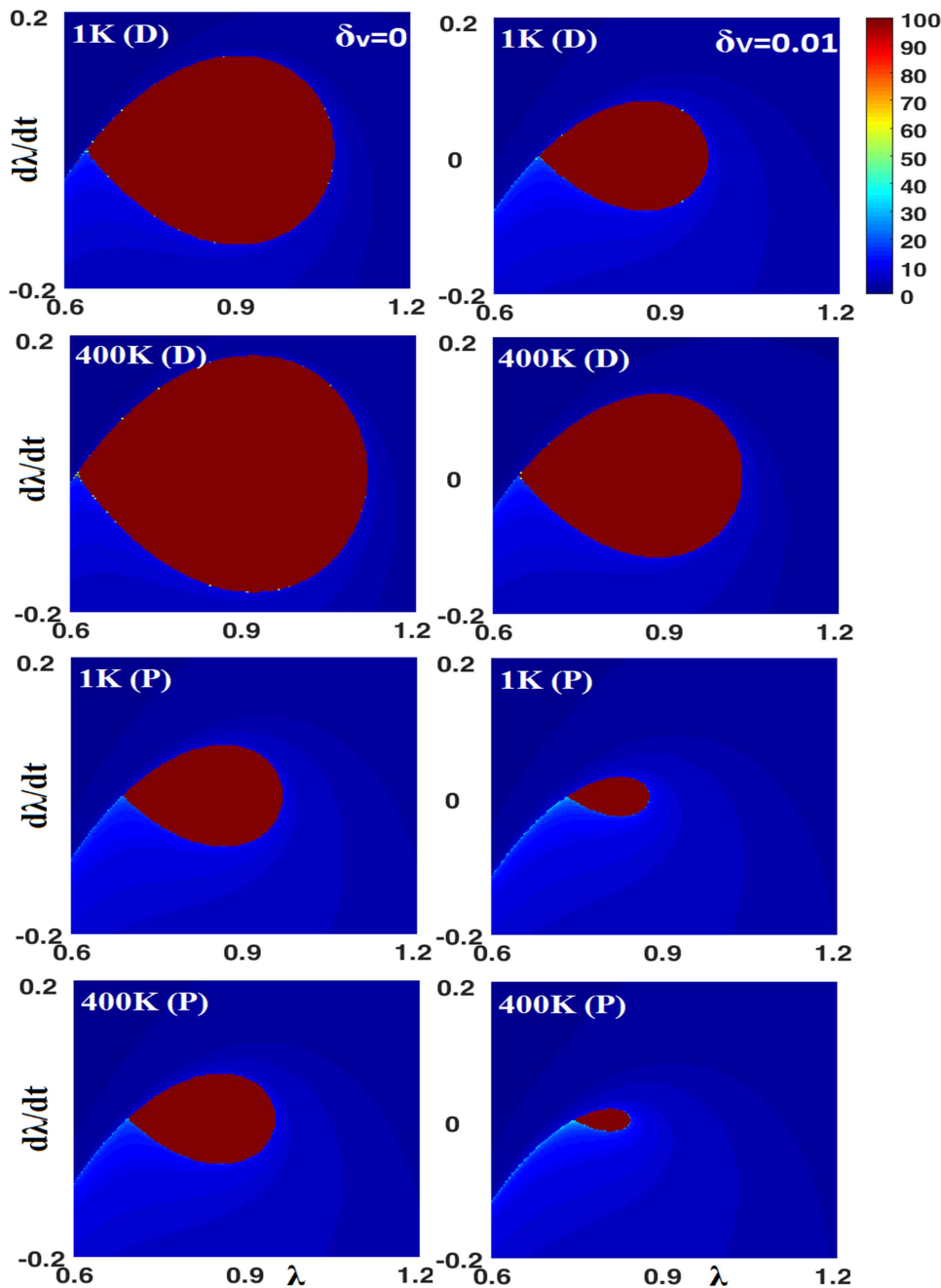


FIG. 6. Contour phase space plots $d\lambda/dt$ vs λ for the Au–Au system. For the calculations, we used 200×200 initial conditions $(\lambda, d\lambda/dt)$. The elliptical homoclinic orbit encloses the initial conditions that lead to stable oscillations. $\delta_{\text{Cas}} = 0.06$ and $d = 2 \mu\text{m}$: $\delta_v = 0$ (left column) and $\delta_v = 0.012$ (right column) using both the Drude and plasma models. Here, we considered $T_1 = 300 \text{ K}$ and $T_2 = 1 \text{ K}$ or 400 K as indicated.

δ_{Cas} , Eq. (5) assumes the more convenient form

$$\frac{d^2\lambda}{dT^2} + \left(\frac{1}{Q}\right) \frac{d\lambda}{dT} = -(1 - \lambda) + \delta_v \frac{F_{\text{elec}}}{F_{\text{elec}}^{\text{m}}} + \delta_{\text{Cas}} \frac{F_{\text{Cas}}}{F_{\text{Cas}}^{\text{m}}} + \epsilon \frac{F_0}{F_{\text{res}}^{\text{Max}}} \cos\left(\frac{\omega}{\omega_0} T\right), \quad (7)$$

with $\lambda = z/d$ and $T = \omega_0 t$.

Casimir force and actuation for good conductivity microsystms (Au–Au): According to Figs. 2(a) and 3(a), the extrapolation with the Drude model at low frequencies results in a large thermal correction for the Au–Au system, which does not occur for the plasma model. The predicted thermal correction of the Drude model has a significant value even at shorter separations ($< 1 \mu\text{m}$). Although several experimental studies are in disagreement with the Drude model’s predictions,^{4,39} there are investigations that show

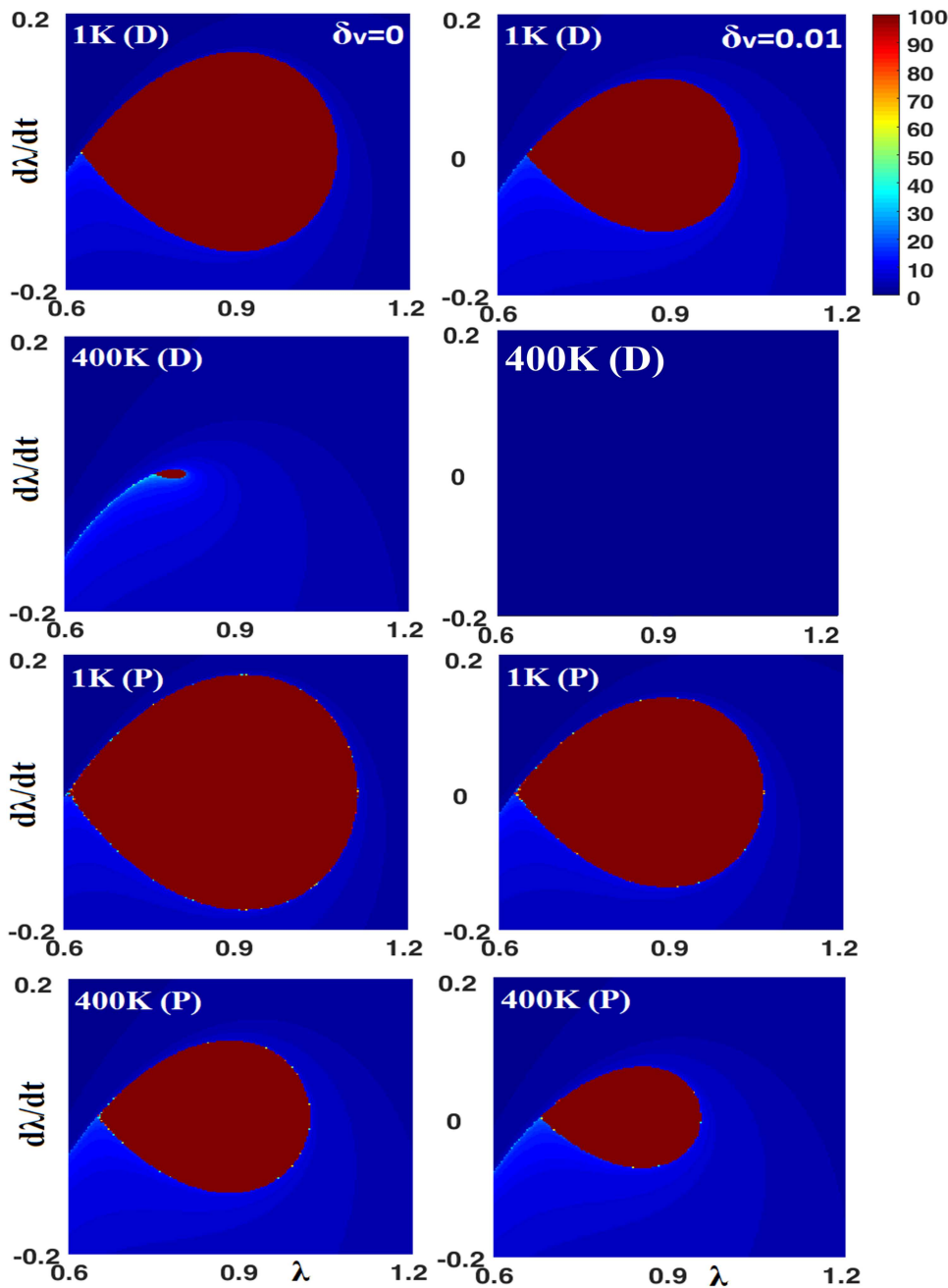


FIG. 7. Contour phase space plots $d\lambda/dt$ vs λ for the SiC-SiC system. For the calculations, we used 200×200 initial conditions $(\lambda, d\lambda/dt)$. The elliptical homoclinic orbit encloses the initial conditions that lead to stable oscillations. $\delta_{Cas} = 0.06$ and $d = 2 \mu\text{m}$: $\delta_v = 0$ (left column) and $\delta_v = 0.012$ (right column) using both the Drude and plasma models. Here, we considered $T_1 = 300 \text{ K}$ and $T_2 = 1 \text{ K}$ or 400 K as indicated.

agreement with the Drude model predictions.⁴⁰ Moreover, the thermal correction is opposite in sign to the main contribution in the Casimir force from zero-point fluctuations (F_0) within a wide range of separations and consequently leads to a decrease in magnitude of the total Casimir force. From Fig. 3(a), for the Drude model, and ignoring the sign of the thermal correction, F_{thermal} becomes weak with the decreasing temperature. The same takes place also for the plasma model, but the sign of F_{thermal} remains positive for

most of the separations. For the good conductive Au-Au system, at large separations ($>4 \mu\text{m}$), the key factor that affects the strength of the thermal contribution is the magnitude of the temperature, while for smaller separations ($<2.5 \mu\text{m}$), the influence of the optical properties at low frequencies overcomes the effect of the magnitude of the temperature.

Finally, Fig. 4(a) provides a comparison between thermal equilibrium and nonequilibrium situations for both the Drude and

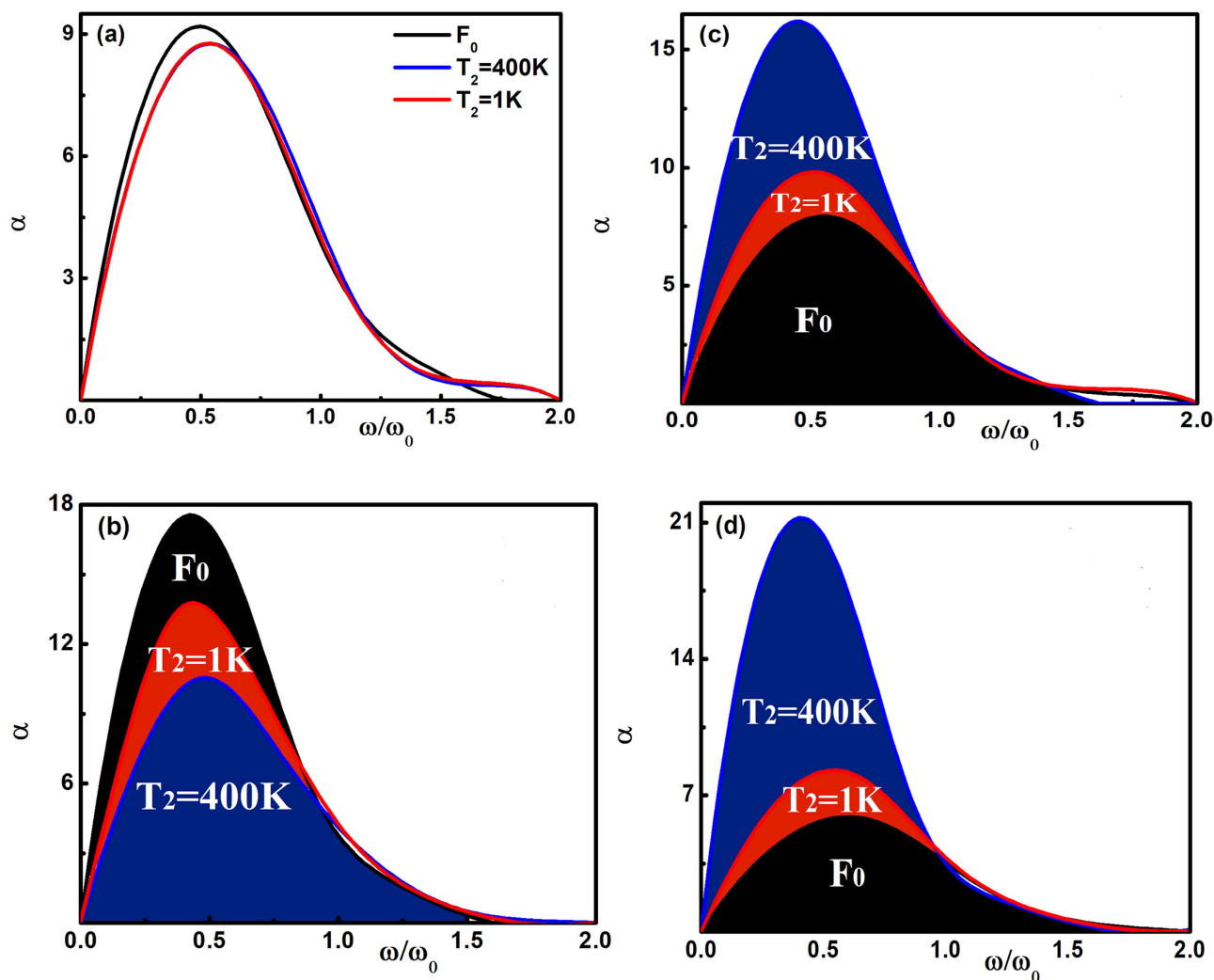


FIG. 8. Threshold curve $\alpha (= \gamma\omega_0 d/F_0)$ vs driving frequency ω/ω_0 (with ω_0 being the natural frequency of the system) to compare the influence of zero-point fluctuations and thermal effects under nonequilibrium conditions with $T_1 = 300$ K, $T_2 = 1$ K or 400 K for the Au–Au system with $\delta_{\text{Cas}} = 0.07$, $\delta_v = 0$, and $d = 1 \mu\text{m}$: (a) plasma model and (b) Drude model. Similar plots are shown for the SiC–SiC system with $\delta_{\text{Cas}} = 0.06$, $\delta_v = 0$, and $d = 1 \mu\text{m}$: (c) plasma model and (d) Drude model.

plasma models vs temperature. For the Drude model, the magnitude of the total Casimir force is stronger for systems at thermal equilibrium for temperatures below 300 K. While for the plasma model below 300 K, the effect of the thermal part is too weak without any difference between thermal equilibrium and nonequilibrium situations. However, by increasing T_2 and consequently strengthening the contribution of the thermal component, the magnitude of total Casimir force becomes stronger at equilibrium conditions, which is the opposite for the Drude model.

Furthermore, Figs. 5(a)–5(c) illustrate the stability of the microsystem operating with different initial separations d . If the restoring force is strong enough ($\delta_{\text{Cas}} < \delta_{\text{Cas}}^{\text{Max}}$), then there are two equilibria for the system. The stationary points closest to d are the

stable centers around which periodic solutions exist, while the points closer to the fixed plate are unstable saddle points so that motion around them will lead to stiction on the fixed plate due to stronger Casimir forces. Considering the negative sign of F_{thermal} in the Drude model, and increasing its magnitude by increasing the temperature, the stability of the system will increase at higher temperatures (e.g., a system at 1 K loses its stability sooner than at 400 K). However, for the plasma model, the thermal effect is negligible at short separations and will not change the device operation. As the initial separation increases, because of the positive contribution of the thermal effect to the Casimir force, the stability of the system will decrease with increasing temperature (e.g., a system at 400 K loses its stability sooner than at 1 K).

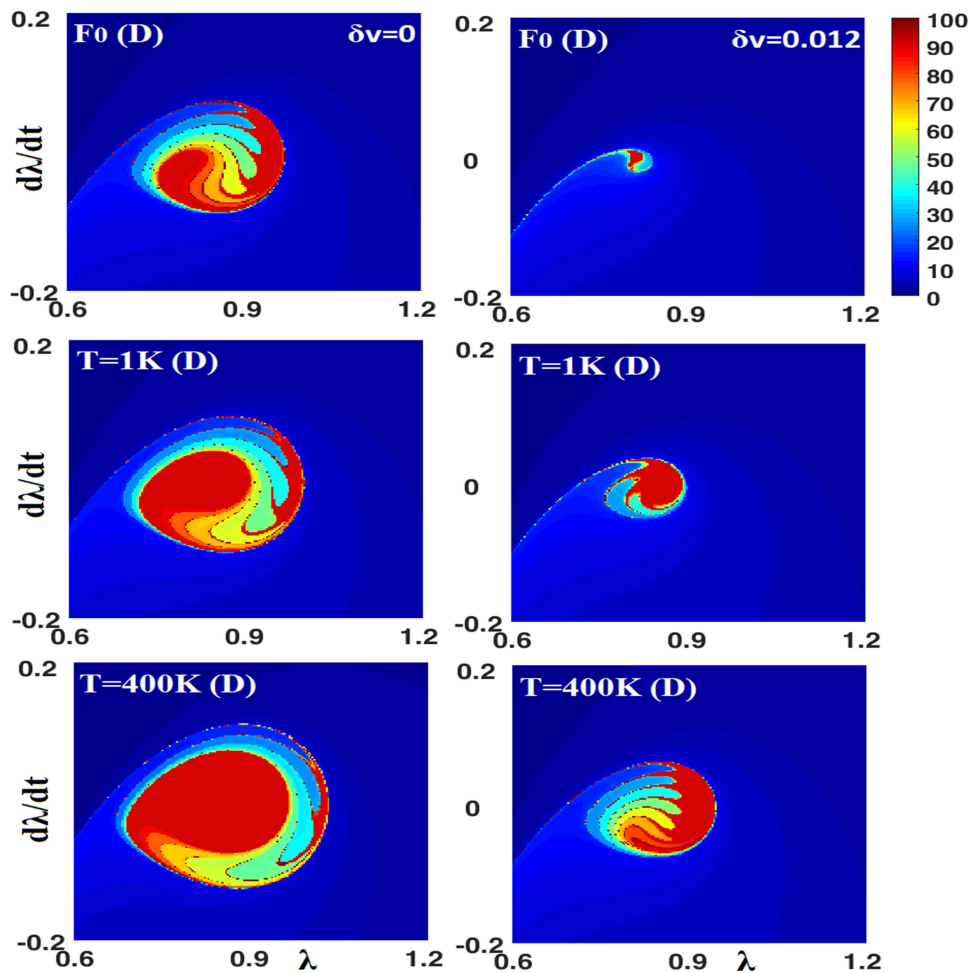


FIG. 9. Contour plot of the transient times to stiction using Poincaré phase maps $d\lambda/dt$ vs λ for the nonconservative Au–Au system using the Drude model with $d = 1 \mu\text{m}$, $\alpha = 0.5$, $\omega/\omega_0 = 0.6$, $\delta_{\text{Cas}} = 0.07$, and $\delta_v = 0$ (left column) and $\delta_v = 0.012$ (right column). In both cases, we also considered the effect of zero-point fluctuations (F_0) and the nonequilibrium effects for $T_1 = 300$ and $T_2 = 1$ K or 400 K (shown in the plots). For the calculations, we used 200×200 initial conditions ($\lambda, d\lambda/dt$).

Besides the bifurcation diagrams, the sensitive dependence of the actuation dynamics on the thermal effect is reflected by the Poincaré maps in Fig. 6. For the conservative system, the homoclinic orbit separates unstable motion, leading to stiction within one period, from the periodic closed orbits around the stable center point. Due to the negative sign of the thermal component in the Au–Au system, if we use the Drude model, which leads to the decrement of the total force, the stable area (elliptical in shape red area) increases by increasing temperature in the absence of any applied voltage. However, by applying a voltage, the effect of the positive effect of the thermal component can be counterbalanced leading to the reduced stable region. On the other hand, for the plasma model (at separations $> 2 \mu\text{m}$), the positive contribution to the Casimir force of the thermal component leads to reduction of the stable operating area, and this effect is amplified by an additional nonzero electrostatic voltage contributing an extra attractive force between the interacting plates.

Casimir force and actuation for poor conductivity microsystems (SiC–SiC): For this system, the thermal effects can generate considerably more significant changes in the Casimir force and, therefore,

into device motion in comparison to the high conductivity materials. As shown in Fig. 3(b), unlike the Au–Au system, here for both the Drude and plasma models, the thermal component for the most range of separations has a positive sign and it increases the magnitude of the Casimir force. The key factor that determines the strength of the thermal effect is the magnitude of the temperature, and its effect is stronger than the influence of the low optical frequencies (using either the Drude or the plasma model for extrapolation). Figure 4(b) indicates the opposite results to those for the Au–Au microsystem if we compare the thermal equilibrium and nonequilibrium situations. The total Casimir force is stronger for the Drude model and also, at low temperature, the magnitude of total Casimir force is in any case stronger for nonequilibrium conditions for both the Drude and plasma modes.

Figures 5(d)–5(f) illustrate the changes of stability for the SiC–SiC system due to the thermal contributions. Unlike to the Au–Au system, for the SiC–SiC system, both the Drude and plasma models generate significant influence in the bifurcation diagrams, where the temperature difference plays a dominant role. As a result, decrement of the temperature leads to increased stable operation

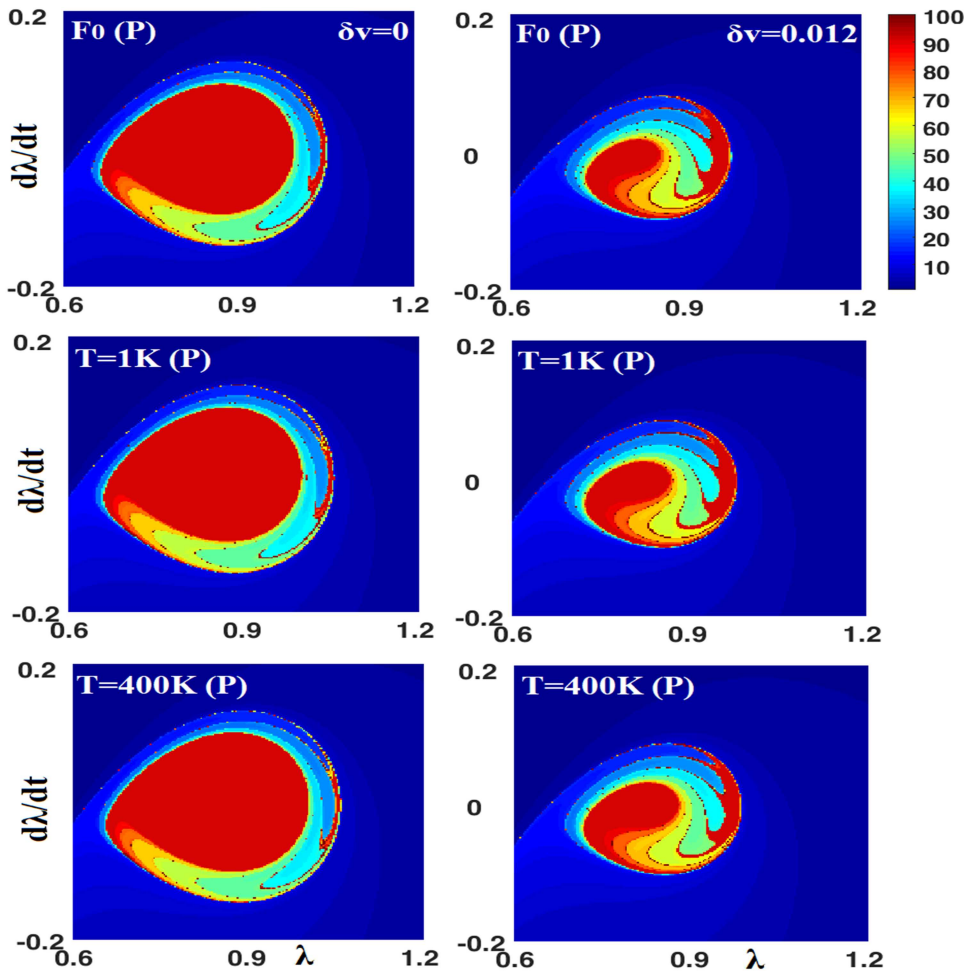


FIG. 10. Contour plot of the transient times to stiction using Poincaré phase maps $d\lambda/dt$ vs λ for the non-conservative Au–Au system using the plasma model with $d = 1 \mu\text{m}$, $\alpha = 0.5$, $\omega/\omega_0 = 0.6$, $\delta_{\text{Cas}} = 0.07$, and $\delta_v = 0$ (left column) and $\delta_v = 0.012$ (right column). In both cases, we also considered the effect of zero-point fluctuations (F_0) and the nonequilibrium effects for $T_1 = 300$, and $T_2 = 1 \text{ K}$ or 400 K (shown in the plots). For the calculations, we used 200×200 initial conditions ($\lambda, d\lambda/dt$).

region as the comparison for 1 K and 400 K operations indicates. Furthermore, we illustrate the dynamical behavior using Poincaré maps. Indeed, Fig. 7 illustrates that, by increasing the temperature, the stable region (elliptical red area) decreases, and the sensitivity to temperature changes is higher for the Drude model. This is due to the extrapolation in low frequencies of the dielectric function for real frequencies, which is the vital input for the calculation of the thermal component. On the other hand, there is no extrapolation for the plasma model at real frequencies, and consequently the influence of the low frequency range on the thermal component is absent. As a result in each column of Fig. 7 (for systems at the same temperature), the stable area is smaller for the Drude model, and the change in stable area is sharper at $T = 400 \text{ K}$ by switching from the Drude to plasma models. Despite the same scenario with the Au–Au system regarding the extrapolations at low frequencies, the reverse behavior takes place for the SiC–SiC system because of the opposite sign of the thermal component in comparison to F_0 in the Drude model for the Au–Au system (leading to larger phase space area for stable Au–Au actuation).

B. Nonconservative systems ($\epsilon = 1$)

Here, we performed calculations to investigate the existence of chaotic behavior in microsystems undergoing forced oscillation via an applied external force $F_0 \cos(\omega t)$ ⁴¹ and compare the influence of thermal effects for both the Drude and plasma models. Chaotic behavior could occur if the separatrix (homoclinic orbit) of the conservative system splits. This behavior can be addressed by the so-called Melnikov function and Poincaré map analysis.^{41,42} In a driven system, the unstable equilibrium turns into an unstable periodic orbit. If we define the homoclinic solution of the conservative system as $\varphi_{\text{hom}}^{\text{C}}(T)$, then the Melnikov function for the oscillating system is given by^{41,42}

$$M(T_0) = \frac{1}{Q} \int_{-\infty}^{+\infty} \left(\frac{d\varphi_{\text{hom}}^{\text{C}}(T)}{dT} \right)^2 dT + \frac{\tau_0}{\tau_{\text{res}}^{\text{MAX}}} \int_{-\infty}^{+\infty} \frac{d\varphi_{\text{hom}}^{\text{C}}(T)}{dT} \cos \times \left[\frac{\omega}{\omega_0} (T + T_0) \right] dT. \tag{8}$$

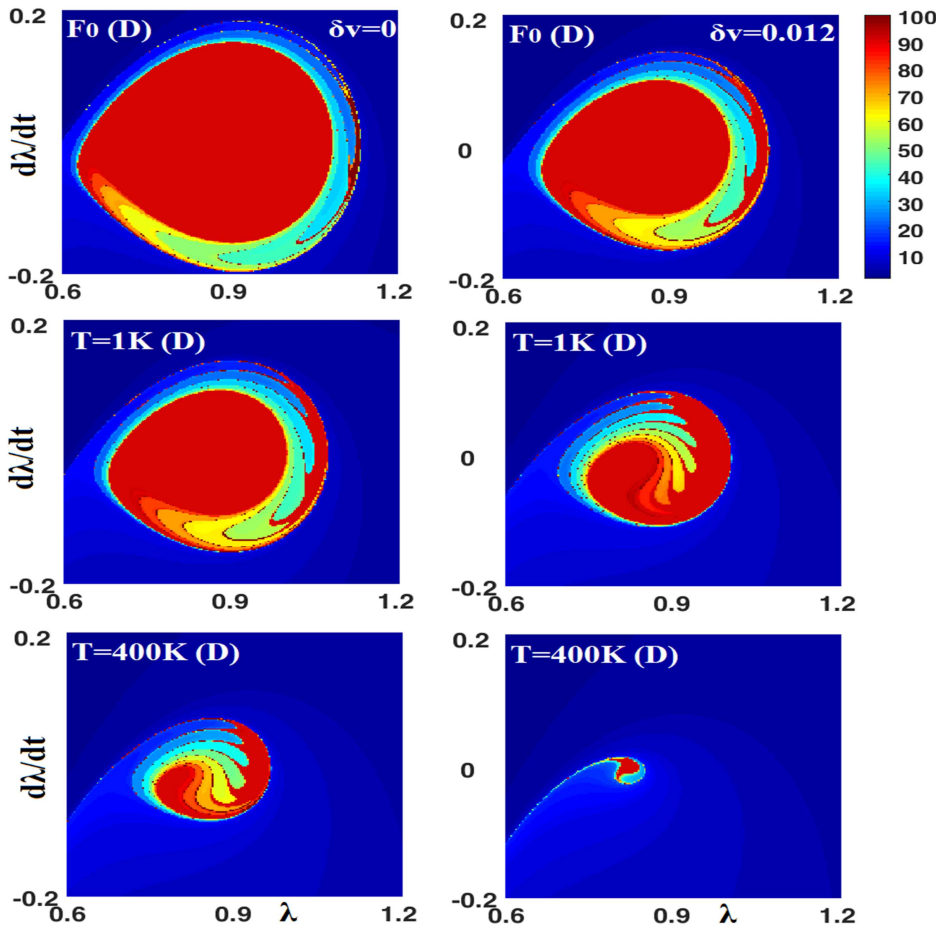


FIG. 11. Contour plot of the transient times to stiction using Poincaré phase maps $d\lambda/dt$ vs λ for the nonconservative SiC-SiC system using the Drude model with $d = 1 \mu\text{m}$, $\alpha = 0.5$, $\omega/\omega_0 = 0.6$, $\delta_{\text{Cas}} = 0.055$ and $\delta_v = 0$ (left column) and $\delta_v = 0.012$ (right column). In both cases, we also considered the effect of zero-point fluctuations (F_0), and the nonequilibrium effects for $T_1 = 300$ and $T_2 = 1 \text{ K}$ or 400 K (shown in the plots). For the calculations, we used 200×200 initial conditions $(\lambda, d\lambda/dt)$.

The separatrix splits if the Melnikov function has simple zeros so that $M(T_0) = 0$ and $M'(T_0) = 0$, while if $M(T_0)$ has no zeros, the motion will not be chaotic. Therefore, the conditions of nonsimple zeros, $M(T_0) = 0$ and $M'(T_0) = 0$, give the threshold condition for chaotic motion.^{41,42} If we define

$$\mu_{\text{hom}}^c = \int_{-\infty}^{+\infty} \left(\frac{d\varphi_{\text{hom}}^c(T)}{dT} \right)^2 dT \quad \text{and} \quad \beta(\omega) = \left| H \left[\text{Re} \left(F \left\{ \frac{d\varphi_{\text{hom}}^c(T)}{dT} \right\} \right) \right] \right|, \quad (9)$$

then the threshold condition for chaotic motion $\alpha = \beta(\omega)/\mu_{\text{hom}}^c$ with $\alpha = (1/Q)(F_0/F_{\text{res}}^{\text{MAX}})^{-1} = \gamma\omega_0 d/F_0$ obtains the form

$$\alpha = \frac{\gamma\omega_0 d}{F_0} = \left| H \left[\text{Re} \left(F \left\{ \frac{d\varphi_{\text{hom}}^c(T)}{dT} \right\} \right) \right] \right| / \int_{-\infty}^{+\infty} \left(\frac{d\varphi_{\text{hom}}^c(T)}{dT} \right)^2 dT, \quad (10)$$

with $\gamma = I\omega_0/Q$ and $H[\dots]$ denotes the Hilbert transform.^{41,42}

Figure 8 shows the threshold curves $\alpha = \gamma\omega_0 d/F_0$ vs driving frequency ratio ω/ω_0 . For large values of α (above the threshold curve), the dissipation dominates the driving force ($\alpha \sim \gamma/F_0$) leading to motion, which asymptotically approaches the stable periodic orbit of the conservative system ($\varepsilon = 0$). However, for parameter values α below the threshold curve, the splitting of the separatrix could lead to chaotic motion. Clearly, for the Au-Au system (good conductors), the thermal contribution calculated via the plasma model [Fig. 8(a)] is not able to change the stability of device since the curves with and without thermal fluctuation are similar to each other. However, for the Drude model [Fig. 8(b)], the thermal contribution decreases the possibility for chaotic motion, which is further augmented by increasing in magnitude of the temperature difference between the actuating components. Furthermore, according to Figs. 8(c) and 8(d), for the SiC-SiC system (poor conductors), the contribution of the thermal component for both the Drude and plasma models can change the occurrence of chaotic behavior. The extrapolation at low frequencies with the Drude model has a stronger effect on the threshold condition for chaotic behavior, which is enhanced by increasing temperature difference between the actuating components.

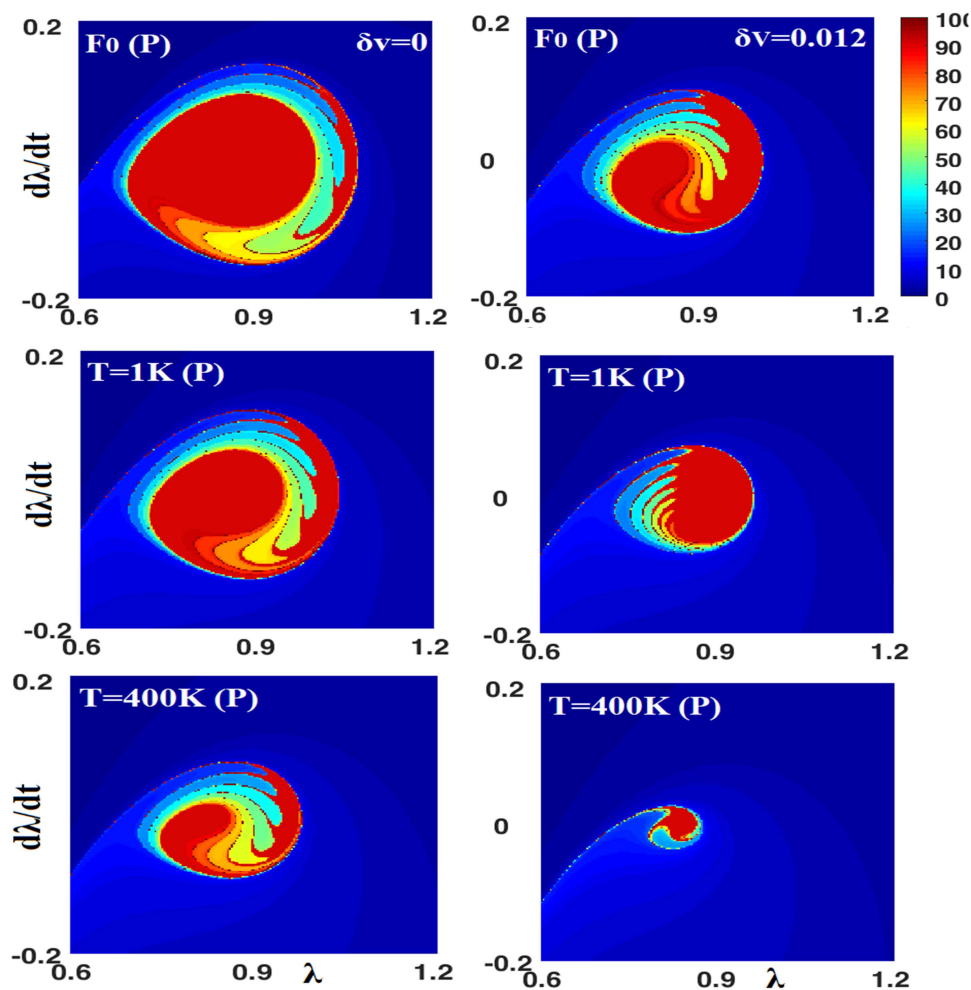


FIG. 12. Contour plot of the transient times to stiction using Poincaré phase maps $d\lambda/dt$ vs λ for the non-conservative SiC-SiC system using the plasma model with $d = 1 \mu\text{m}$, $\alpha = 0.5$, $\omega/\omega_0 = 0.6$, $\delta_{\text{Cas}} = 0.055$ and $\delta_v = 0$ (left column) and $\delta_v = 0.012$ (right column). In both cases, we considered also the effect of zero-point fluctuations (F_0) and the nonequilibrium effects for $T_1 = 300$ and $T_2 = 1$ K or 400 K (shown in the plots). For the calculations, we used 200×200 initial conditions (λ , $d\lambda/dt$).

The occurrence of chaotic motion can be confirmed by investigating the sensitive dependence of the motion on its initial conditions via the Poincaré maps, as shown in Figs. 9–12. When the possibility for chaotic motion to occur increases with a decreasing value of α from the Melnikov analysis, there is a region of initial conditions where the distinction between qualitatively different solutions is unclear. For chaotic motion, there is no simple smooth boundary between the red (lighter gray) and the blue (dark gray) regions (as it is the case for conservative motion in Figs. 6 and 7). As a result, if the motion is chaotic, then stiction can still take place after several periods affecting the long-term stability of the device. Therefore, chaotic behavior introduces significant risk for stiction, and this is more prominent to occur when the magnitude of the Casimir force increases limiting our ability to predict the long-term behavior of the actuating systems.

For the Au-Au system, if we compare the Poincaré maps of Fig. 9 (Drude model) and Fig. 10 (plasma model), it is evident that for the Drude model, the thermal corrections are more effective to suppress the occurrence of chaotic motion and enhance stable actuation with further increment of the temperature difference. At the

same time, the presence of an electrostatic voltage can reduce or even fully compensate the positive effect of the thermal component and subsequently drive the system to chaotic motion and stiction. On the other hand, for the plasma model, the effect of the thermal contribution is rather weak to alter the chaotic behavior in the presence or absence of any electrostatic forces. According to Figs. 11 and 12, for the SiC-SiC system, the thermal contributions for both the Drude and plasma models are able to make significant changes in the dynamics of the actuating system toward chaotic motion. By comparing the Poincaré maps in Figs. 11 and 12, it is obvious that the strength of the thermal contribution is higher for the Drude model in the absence and/or presence of electrostatic voltage leading to increased chaotic behavior. This is because of the differences in extrapolating at real frequencies between the Drude and plasma models.

IV. CONCLUSIONS

In conclusion, we investigated the sensitivity of nonequilibrium Casimir forces to optical properties at low frequencies via the Drude

and plasma models during actuation of microsystems. For the latter, we explored how the thermal effects influence the stable and chaotic motion for both autonomous conservative and nonconservative driven systems assuming both good and poor conductors, whose static conductivity is different by more than three orders of magnitude. For both material systems, we used the Drude and plasma models to extrapolate the optical properties at low frequencies, where optical measurements are not feasible. In fact, for the conservative actuating system, bifurcation and phase space analysis show that the system motion is strongly influenced by the thermal nonequilibrium effects depending on the modeling of the optical properties at low frequencies, where also the presence of residual electrostatic forces can drastically alter the actuating state of the system, depending strongly on the material conductivity. For non-conservative systems, the Melnikov function approach is used to explore the possible presence of chaotic motion rendering predictions of stable actuation or malfunction due to stiction over long times rather impossible. Moreover, it is shown that the thermal contributions produce the opposite effect for the emerging chaotic behavior of the Au–Au and SiC–SiC systems, if the Drude model is used to model the low optical frequencies. On the other hand, when using the plasma model only for the poor conducting SiC–SiC system, the possibility of chaotic motion is enhanced, while for the good conducting Au–Au system at small separations (less than $2\ \mu\text{m}$), the chaotic behavior will remain unaffected. Therefore, the modeling of the low frequency regime for the materials under consideration in combination with thermal effects, and applied (or uncompensated) electrostatic voltages, must be taken very carefully into account for the design of actuating devices.

ACKNOWLEDGMENTS

G.P. and Z.B. acknowledge support from the Netherlands Organization for Scientific Research (NWO) under Grant No. 16PR3236. F.T. and A.A.M. acknowledge support from the Department of Physics at the Alzakra University. We would also like to thank V. B. Svetovoy from the Zernike Institute of Advanced Materials and H. Waalkens from the Bernoulli Institute for Mathematics, Computer Science and Artificial Intelligence, University of Groningen, for useful discussions.

APPENDIX A: LIFSHITZ THEORY AND DIELECTRIC FUNCTION OF MATERIALS WITH EXTRAPOLATIONS

The part of the Casimir force due to zero-point fluctuations (F_0) in Eq. (5) is given by¹¹

$$F_{\text{Cas}}(d) = \frac{\hbar}{2\pi^2} \int_0^\infty d\xi \int_0^\infty dk_\perp k_\perp k_0 \sum_{\nu=\text{TE, TM}} \frac{r_\nu^{(1)} r_\nu^{(2)} \exp(-2k_0 d)}{1 - r_\nu^{(1)} r_\nu^{(2)} \exp(-2k_0 d)}. \tag{A1}$$

The Fresnel reflection coefficients are given by $r_{\text{TE}}^{(i)} = (k_0 - k_i)/(k_0 + k_i)$ and $r_{\text{TM}}^{(i)} = (\epsilon_i k_0 - \epsilon_0 k_i)/(\epsilon_i k_0 + \epsilon_0 k_i)$ for the transverse electric (TE) and magnetic (TM) field polarizations, respectively. $k_i (i = 0, 1, 2) = \sqrt{\epsilon_i(i\xi_1) + k_\perp^2}$ represents the out-of-plane wave vector in the gap between the interacting plates (k_0)

and in each of the interacting plates ($k_{i=(1,2)}$). k_\perp is the in-plane wave vector. The function $\epsilon(i\xi)$ is the dielectric function evaluated at imaginary frequencies (ξ), which is the necessary input for calculating the Casimir force between real materials using the Lifshitz theory. The latter is given by¹¹

$$\epsilon(i\xi) = 1 + \frac{2}{\pi} \int_0^\infty \frac{\omega \epsilon''(\omega)}{\omega^2 + \xi^2} d\omega. \tag{A2}$$

For the calculation of the integral in Eq. (A2), one needs the measured data for the imaginary part $\epsilon''(\omega)$ of the frequency dependent dielectric function $\epsilon(\omega)$. The materials were optically characterized by ellipsometry over a wide range of frequencies at J. A. Woollam Co. using the VUV-VASE (0.5–9.34 eV) and IR-VASE (0.03–0.5 eV).^{19,24,31}

In any case, the experimental data for the imaginary part $\epsilon''(\omega)$ of the dielectric function cover only a limiting range of frequencies $\omega_1 (=0.03\ \text{eV}) < \omega < \omega_2 (=8.9\ \text{eV})$. Therefore, for the low optical frequencies ($\omega < \omega_1$), we extrapolated using the imaginary part of the Drude model^{19,24,31}

$$\epsilon''_{\text{L}}(\omega) = \frac{\omega_p^2 \omega_\tau}{\omega (\omega^2 + \omega_\tau^2)}, \tag{A3}$$

where ω_p is the plasma frequency and ω_τ is the relaxation frequency. Furthermore, for the high optical frequencies ($\omega > \omega_2$), we extrapolated using^{17,19,24,31}

$$\epsilon''_{\text{H}}(\omega) = \frac{A}{\omega^3}. \tag{A4}$$

Finally, using Eqs. (A2)–(A4), $\epsilon(i\xi)$ is given by

$$\epsilon(i\xi) D = 1 + \frac{2}{\pi} \int_{\omega_1}^{\omega_2} \frac{\omega \epsilon''_{\text{exp}}(\omega)}{\omega^2 + \xi^2} d\omega + \Delta_{\text{L}}\epsilon(i\xi) + \Delta_{\text{H}}\epsilon(i\xi), \tag{A5}$$

with

$$\Delta_{\text{L}}\epsilon(i\xi) = \frac{2}{\pi} \int_0^{\omega_1} \frac{\omega \epsilon''_{\text{L}}(\omega)}{\omega^2 + \xi^2} d\omega, \text{ and } \Delta_{\text{H}}\epsilon(i\xi) = \frac{2}{\pi} \int_{\omega_2}^\infty \frac{\omega \epsilon''_{\text{H}}(\omega)}{\omega^2 + \xi^2} d\omega. \tag{A6}$$

Despite the lack of a strong physical background in the plasma model, Casimir force calculation by means of the plasma model have better agreement with experimental force data than the Drude model. At low optical frequencies $\omega < \omega_1$, the term $\Delta_{\text{L}}\epsilon(i\xi)$ from the Drude model is replaced by ω_p^2/ζ^2 yielding³¹

$$\epsilon(i\xi)_p = 1 + \frac{2}{\pi} \int_{\omega_1}^{\omega_2} \frac{\omega \epsilon''_{\text{exp}}(\omega)}{\omega^2 + \xi^2} d\omega + \frac{\omega_p^2}{\zeta^2} + \Delta_{\text{H}}\epsilon(i\xi). \tag{A7}$$

APPENDIX B: BRIEF THEORY OF THE NONEQUILIBRIUM CASIMIR FORCE

As already shown in Ref. 25, for identical materials, the antisymmetric parts of both the propagating and evanescent components vanish, while their symmetric parts remain equal to equilibrium terms. Therefore, the z-dependent terms of the thermal force

in a system with identical bodies at T_1 and T_2 can be written as

$$F_{\text{th}}^{\text{eq}}(T_1, T_2, z) = \frac{1}{2} \left[F_{\text{th}}^{\text{eq}, \text{PW}}(T_1, 0, z) + F_{\text{th}}^{\text{eq}, \text{EW}}(T_1, 0, z) \right] + \frac{1}{2} \left[F_{\text{th}}^{\text{eq}, \text{PW}}(0, T_2, z) + F_{\text{th}}^{\text{eq}, \text{EW}}(0, T_2, z) \right], \quad (\text{B1})$$

where for the propagating component we have

$$F_{\text{th}}^{\text{eq}, \text{PW}}(T, z) = \frac{-\hbar}{\pi^2} \int_0^\infty d\kappa \frac{1}{\exp\left(\frac{\hbar\omega}{k_B T}\right) - 1} \int_0^k dk_\perp k_\perp k_0 \sum_{v=s,p} \times \frac{\text{Re}(r_1^v r_2^v \exp(2id k_0 z)) - |r_1^v r_2^v|^2}{|D_v|^2}, \quad (\text{B2})$$

while for the evanescent component we have

$$F_{\text{th}}^{\text{eq}, \text{EW}}(T, z) = \frac{\hbar}{\pi^2} \int_0^\infty d\omega \frac{1}{\exp\left(\frac{\hbar\omega}{k_B T}\right) - 1} \int_k^\infty dk_\perp k_\perp \text{Im}(k_0) \times \exp(-2d \text{Im}(k_0 z)) \sum_{v=\text{TE}, \text{T}} \frac{\text{Im}(r_1^v r_2^v)}{|D_v|^2}. \quad (\text{B3})$$

Equations (B1)–(B3) describe the force per unit area, with ω being the real frequency and $D_v = 1 - r_1^v r_2^v \exp(2i k_0 z)$. Both coefficients r_1^v and r_2^v are defined in Appendix A with $k_i (i = 0, 1, 2) = (\epsilon_i(\omega)(\omega^2/c^2) + k_\perp^2)^{1/2}$ and $\epsilon(\omega) = \epsilon_{\text{real}}(\omega) + i\epsilon_{\text{imag}}(\omega)$.

REFERENCES

- ¹A. W. Rodriguez, F. Capasso, and S. G. Johnson, “The Casimir effect in microstructured geometries,” *Nat. Photonics* **5**, 211 (2011).
- ²F. Capasso, J. N. Munday, D. Iannuzzi, and H. B. Chan, “Casimir forces and quantum electrodynamic torques: Physics and nanomechanics,” *IEEE J. Sel. Top. Quantum Electron.* **13**, 400 (2007).
- ³M. Bordag, G. L. Klimchitskaya, U. Mohideen, and V. M. Mostepanenko, *Advances in the Casimir Effect* (Oxford University Press, New York, 2009).
- ⁴R. S. Decca, D. Lopez, E. Fischbach, G. L. Klimchitskaya, D. E. Krause, and V. M. Mostepanenko, “Precise comparison of theory and new experiment for the Casimir force leads to stronger constraints on thermal quantum effects and long-range interactions,” *Ann. Phys.* **318**, 37 (2005); R. S. Decca, D. Lopez, E. Fischbach, G. L. Klimchitskaya, D. E. Krause, and V. M. Mostepanenko, “Tests of new physics from precise measurements of the Casimir pressure between two gold-coated plates,” *Phys. Rev. D* **75**, 077101 (2007).
- ⁵A. Ashourvan, M. F. Miri, and R. Golestanian, “Noncontact rack and pinion powered by the lateral Casimir force,” *Phys. Rev. Lett.* **98**, 140801 (2007).
- ⁶M. F. Miri and R. Golestanian, “A frustrated nanomechanical device powered by the lateral Casimir force,” *Appl. Phys. Lett.* **92**, 113103 (2008).
- ⁷A. Ashourvan, M. F. Miri, and R. Golestanian, “Rectification of the lateral Casimir force in a vibrating noncontact rack and pinion,” *Phys. Rev. E* **75**, 040103 (2007).
- ⁸F. M. Serry, D. Walliserand, and G. J. Maclay, “The role of the Casimir effect in the static deflection and stiction of membrane strips in microelectromechanical systems (MEMS),” *J. Appl. Phys.* **84**, 2501 (1998); F. M. Serry, D. Walliserand, and G. J. Maclay, “The anharmonic Casimir oscillator (ACO)—The Casimir effect in a model microelectromechanical system,” *J. Microelectromech. Syst.* **4**, 193 (1995); G. Palasantzas and J. T. M. DeHosson, “Phase maps of microelectromechanical switches in the presence of electrostatic and Casimir forces,” *Phys. Rev. B* **72**, 121409 (2005); G. Palasantzas and J. T. M. DeHosson, “Pull-in characteristics of electromechanical switches in the presence of Casimir forces: Influence of self-affine surface roughness,” *ibid.* **72**, 115426 (2005).

- ⁹F. W. DelRio, M. P. de Boer, J. A. Knapp, E. D. Reedy, Jr., P. J. Clews, and M. L. Dunn, “The role of van der Waals forces in adhesion of micromachined surfaces,” *Nat. Mater.* **4**, 629 (2005).
- ¹⁰H. B. G. Casimir, “Zero point energy effects on quantum electrodynamics,” *Proc. K. Ned. Akad. Wet.* **51**, 793 (1948).
- ¹¹E. M. Lifshitz, “The theory of molecular attractive forces between solids,” *J. Exp. Theor. Phys.* **2**, 73 (1956); I. E. Dzyaloshinskii, E. M. Lifshitz, and L. P. Pitaevskii, “General theory of van der Waals forces,” *Sov. Phys. Usp.* **4**, 153 (1961).
- ¹²P. Ball, “Fundamental physics: Feel the force,” *Nature* **447**, 77 (2007).
- ¹³H. G. Craighead, “Nanoelectromechanical systems,” *Science* **290**, 1532 (2000).
- ¹⁴F. Chen, G. L. Klimchitskaya, V. M. Mostepanenko, and U. Mohideen, “Demonstration of optically modulated dispersion forces,” *Opt. Express* **15**, 4823 (2007); G. Torricelli, I. Pirozhenko, S. Thornton, A. Lambrecht, and C. Binns, “Casimir force between a metal and a semimetal,” *Europhys. Lett.* **93**, 51001 (2011).
- ¹⁵S. de Man, K. Heeck, R. J. Wijngaarden, and D. Iannuzzi, “Halving the Casimir force with conductive oxides,” *Phys. Rev. Lett.* **103**, 040402 (2009).
- ¹⁶G. Torricelli, P. J. van Zwol, O. Shpak, C. Binns, G. Palasantzas, B. J. Kooi, V. B. Svetovoy, and M. Wuttig, “Switching Casimir forces with phase-change materials,” *Phys. Rev. A* **82**, 010101(R) (2010).
- ¹⁷G. Torricelli, P. J. van Zwol, O. Shpak, G. Palasantzas, V. B. Svetovoy, C. Binns, B. J. Kooi, P. Jost, and M. Wuttig, “Casimir force contrast between amorphous and crystalline phases of AIST,” *Adv. Funct. Mater.* **22**, 3729 (2012).
- ¹⁸C.-C. Chang, A. A. Banishev, G. L. Klimchitskaya, V. M. Mostepanenko, and U. Mohideen, “Reduction of the Casimir force from indium tin oxide film by UV treatment,” *Phys. Rev. Lett.* **107**, 090403 (2011).
- ¹⁹V. B. Svetovoy, P. J. van Zwol, G. Palasantzas, and J. Th. M. De Hosson, “Optical properties of gold films and the Casimir force,” *Phys. Rev. B* **77**, 035439 (2008); G. Bimonte, “Making precise predictions of the Casimir force between metallic plates via a weighted Kramers-Kronig transform,” *Phys. Rev. A* **83**, 042109 (2011).
- ²⁰A. Canaguier-Durand, P. A. Maia Neto, A. Lambrecht, and S. Reynaud, “Thermal Casimir effect for Drude metals in the plane-sphere geometry,” *Phys. Rev. A* **82**, 012511 (2010).
- ²¹F. Tajik, M. Sedighi, M. Khorrami, A. A. Masoudi, and G. Palasantzas, “Chaotic behavior in Casimir oscillators: A case study for phase-change materials,” *Phys. Rev. E* **96**, 042215 (2017); F. Tajik, M. Sedighi, and G. Palasantzas, “Sensitivity on materials optical properties of single beam torsional Casimir actuation,” *J. Appl. Phys.* **121**, 174302 (2017).
- ²²F. Tajik, M. Sedighi, M. Khorrami, A. A. Masoudi, H. Waalkens, and G. Palasantzas, “Dependence of chaotic behavior on optical properties and electrostatic effects in double-beam torsional Casimir actuation,” *Phys. Rev. E* **98**, 02210 (2018).
- ²³M. Sedighi and G. Palasantzas, “Casimir and hydrodynamic force influence on microelectromechanical system actuation in ambient conditions,” *Appl. Phys. Lett.* **104**, 074108 (2014).
- ²⁴M. Sedighi, V. B. Svetovoy, W. H. Broer, and G. Palasantzas, “Casimir forces from conductive silicon carbide surfaces,” *Phys. Rev. B* **89**, 195440 (2014).
- ²⁵M. Antezza, L. P. Pitaevskii, S. Stringari, and V. B. Svetovoy, “Casimir-Lifshitz force out of thermal equilibrium,” *Phys. Rev. A* **77**, 022901 (2008).
- ²⁶J. M. Obrecht, R. J. Wild, M. Antezza, L. P. Pitaevskii, S. Stringari, and E. A. Cornell, “Measurement of the temperature dependence of the Casimir-Polder force,” *Phys. Rev. Lett.* **98**, 063201 (2007); G. L. Klimchitskaya, V. M. Mostepanenko, and R. I. P. Sedmik, “Casimir pressure between metallic plates out of thermal equilibrium: Proposed test for the relaxation properties of free electrons,” *Phys. Rev. A* **100**, 022511 (2019).
- ²⁷M. Antezza, L. P. Pitaevskii, and S. Stringari, “New asymptotic behavior of the surface-atom force out of thermal equilibrium,” *Phys. Rev. Lett.* **95**, 113202 (2005).
- ²⁸F. Tajik, M. Sedighi, Z. Babamahdi, A. A. Masoudi, H. Waalkense, and G. Palasantzas, “Dependence of non-equilibrium Casimir forces on material optical properties towards chaotic motion during device actuation,” *Chaos* **29**, 093126 (2019).
- ²⁹F. Tajik, M. Sedighi, A. A. Masoudi, H. Waalkense, and G. Palasantzas, “Sensitivity of chaotic behavior to low optical frequencies of a double beam torsional actuator,” *Phys. Rev. E* **100**, 012201 (2019).

- ³⁰C. C. Chang, A. A. Banishev, R. Castillo-Garza, G. L. Klimchitskaya, V. M. Mostepanenko, and U. Mohideen, "Gradient of the Casimir force between Au surfaces of a sphere and a plate measured using an atomic force microscope in a frequency-shift technique," *Phys. Rev. B* **85**, 165443 (2012); H. C. Chiu, G. L. Klimchitskaya, V. N. Marachevsky, V. M. Mostepanenko, and U. Mohideen, "Lateral Casimir force between sinusoidally corrugated surfaces: Asymmetric profiles, deviations from the proximity force approximation, and comparison with exact theory," *ibid.* **81**, 115417 (2010); F. Chen, U. Mohideen, G. L. Klimchitskaya, and V. M. Mostepanenko, "Experimental and theoretical investigation of the lateral Casimir force between corrugated surfaces," *Phys. Rev. A* **66**, 032113 (2002).
- ³¹M. Sedighi and G. Palasantzas, "Influence of low optical frequencies on actuation dynamics of microelectromechanical systems via Casimir forces," *J. Appl. Phys.* **117**, 144901 (2015).
- ³²J. A. Pelesko and D. H. Bernstein, *Modeling MEMS and NEMS* (Chapman & Hall, Boca Raton, FL, 2003).
- ³³R. Garcia and R. Perez, "Dynamic atomic force microscopy methods," *Surf. Sci. Rep.* **47**, 197 (2002); D. Rugar, R. Budakian, H. J. Mamin, and B. W. Chui, "Single spin detection by magnetic resonance force microscopy," *Nature* **430**, 329 (2004).
- ³⁴S. Cui and Y. C. Soh, "An accurate separation estimation algorithm for the Casimir oscillator," *J. Microelectromech. Syst.* **19**, 1153 (2010).
- ³⁵M. Sedighi, W. H. Broer, G. Palasantzas, and B. J. Kooi, "Sensitivity of micromechanical actuation on amorphous to crystalline phase transformations under the influence of Casimir forces," *Phys. Rev. B* **88**, 165423 (2013).
- ³⁶R. Esquivel-Sirvent, L. Reyes, and J. Bárcenas, "Stability and the proximity theorem in Casimir actuated nano device," *New J. Phys.* **8**, 241 (2006).
- ³⁷R. Esquivel-Sirvent, M. A. Palomino-Ovando, and G. H. Cocoletzi, "Pull-in control due to Casimir forces using external magnetic fields," *Appl. Phys. Lett.* **95**, 051909 (2009).
- ³⁸O. Degani, Y. Nemirovsky, and J. Microelectromech, "Design considerations of rectangular electrostatic torsion actuators with rectangular plates based on analytical pull-in expressions," *J. Microelectromech. Syst.* **11**, 20 (2002).
- ³⁹R. S. Decca, D. Lopez, E. Fischbach, G. L. Klimchitskaya, D. E. Krause, and V. M. Mostepanenko, "Novel constraints on light elementary particles and extra-dimensional physics from the Casimir effect," *Eur. Phys. J. C* **51**, 963 (2007); V. A. Yampol'skii, S. Savel'ev, Z. A. Mayselis, S. S. Apostolov, and S. Nori, "Anomalous temperature dependence of the Casimir force for thin metal films," *Phys. Rev. Lett.* **101**, 096803 (2008); I. Brevik, S. A. Ellingsen, and K. A. Milton, "Thermal corrections to the Casimir effect," *New J. Phys.* **8**, 236 (2006).
- ⁴⁰A. O. Sushkov, W. J. Kim, D. A. R. Dalvit, and S. K. Lamoreaux, "Observation of the thermal Casimir force," *Nature* **7**, 230 (2011).
- ⁴¹W. Broer, H. Waalkens, V. B. Svetovoy, J. Knoester, and G. Palasantzas, "Non-linear actuation dynamics of driven Casimir oscillators with rough surfaces," *Phys. Rev. Appl.* **4**, 054016 (2015).
- ⁴²M. W. Hirsch, S. Smale, and R. L. Devaney, *Differential Equations, Dynamical Systems, and an Introduction to Chaos* (Elsevier Academic Press, San Diego, CA, 2004).